Design and Position Control of a Robot with 5 Degrees of Freedom

Henry Peralta-Caprachin, Raul Angeles-Orahulio, and Ernesto Paiva-Peredo *

Faculty of Engineering, Universidad Tecnológica del Perú, Lima, Peru
Email: U17204373@utp.edu.pe (H.P-C.); 1520752@utp.edu.pe (R.A-O.); epaiva@utp.edu.pe (E.P-P.)
*Corresponding author

***Abstract*—In recent decades, robotics and artificial intelligence have gained significant importance for their involvement in various industrial processes currently at their peak. Nevertheless, advanced robots are not designed explicitly for lemon supply. This research aims to develop a manipulator robot with 5 degrees of freedom and control its trajectories for lemon supply purposes. To achieve this goal, kinematic and dynamic calculations of the manipulator robot were performed, along with the development of programming code in Matlab to determine its trajectories, positions, speeds, and accelerations. In addition, the Proportional Integral Derivative (PID) tuner was used to obtain the optimal controller parameters and ensure accurate joint trajectory generation.**

***Keywords*—robotic arm, Proportional Integral Derivative (PID) controller, robot path, control, modeling, human-robot interaction**

I. Introduction

The automated system for lemon juice extraction comprises a complex production line encompassing various stages, including supply, washing and drying, cutting and compression, control, bottling, and labeling processes. Within this production line, the precise and swift execution of tasks is imperative, requiring the involvement of three manipulator robots responsible for tasks such as the supply of raw material, the entry of empty plastic containers, and the retrieval of filled bottles. However, despite the availability of advanced robots equipped with sophisticated controls, none are tailored to the specific task of supplying lemons. In response to this gap, the current research focuses on the designing and controlling of a 5-Degree-of-Freedom (5-DOF) robot dedicated to the lemon supply process. This process includes picking up the container, elevating it to a fixed point, tilting it, and transporting it to the opposite end for orderly release.

To carry out the solution of the problem, first the design of the manipulator robot is developed, consequently its dynamics and kinematics, to finally carry out the respective control and be able to define the correct trajectories of the robot [1–5].

II. Literature Review

Robots are widely used for specific functions that require high levels of precision, strength, balance, and speed, among others. An illustrative instance in medicine is the intelligent robot developed by Bouterra *et al*. [6]. It aims to conduct wrist rehabilitation using a novel muscle evaluation protocol that relies on the Internet of Things (IoT) and extracting electromagnetic (EMG) signals. In the same area, Acuna *et al*. [7] validated a robotic system for the mechanical characterization of soft tissues by a micromanipulator capable of performing tests of 5 nN–50 μN tests.

On the other hand, we have robots that run in real-time, like the one developed by Pinrath and Matsuhira [8]. He designed a semi-autonomous simulator that runs on any unknown narrow path based on Braitenberg and Motion Planning Module (MPL) algorithms. Similarly, Igo designed an optimal robot for going up and down stairs and retrieving objects from complex places. Unlike the previous one, this robot is based on a claw mechanism to obtain a better grip when executing the movements [9].

Currently, there is a wide variety of controls for robots. These vary according to the function it will perform and the designer's approach to it. Yuan *et al.* [10] proposed a new type of robot control called Zafe Control Gym that supports control techniques based on other models or collected data. In contrast, the Robot Operator System (ROS), pioneered by Fischer *et al.* [11], relies on cutting-edge perception and control algorithms, and its programming code is predominantly implemented in C++.

However, there are other groups of complex controls designed for soft robots. Zhou *et al*. [12] developed a control based on an electromechanical dynamic model that adaptively compensates the parameters during the execution of a multilayer flexure actuator. According to the author, the performance of this type of control is superior to that of a Proportional Integral Derivative (PID) control. On the other hand, Weng *et al.* [13] presented a feedback control that ensures improved convergence performance, where the parameterization of the Lyapunov control is done correctly in space.

Manuscript received September 26, 2023; revised November 11, 2023; accepted December 7, 2023; published April 10, 2024.

In the same row of complex controllers, hybrid algorithms like the one developed by Yahya and Abbas [14]. He combined two types of algorithms, the Salp Swarm Algorithm (SSA) and Gray Wolf Optimizer (GWO), thus generating an Integral Slider Mode Controller (ISMC) whose objective was to improve the performance of a 2-link flexible joint manipulator. Instead, Herguez *et al.* [15] developed a control based on double integrator dynamic modeling whose objective was to ensure that the robot does not make excessive collisions or stretches.

However, commonly employed control methods in the industry, chosen for their characteristics and the simplicity of their algorithms, include predictive control. Clitan *et al*. [16] applied this control to a DC motor in an industrial robot manipulator to predict forward and backward motion. In this particular predictive control approach, the Dead Beat algorithm was utilized due to its ability to generate a control structure effortlessly.

Predictive control can also use Long Short-Term Memory (LSTM), developed by Najafqolian *et al*. [17]. He used LSTM to encompass a cascade and position controller to achieve effective UAV training.

Proportional Integral Derivative (PID) control is another type widely used in the industry due to its robustness and wide application. The optimal setting of a PID controller is widely used for manipulator robots and delta parallel robots [18, 19]. It is based on hybrid optimization algorithms and dynamic features that help perform a correct master-slave synchronization [20, 21].

The planning of the movement and the trajectory that the robot will carry out is essential for its correct execution since, in this way, the machine-machine or machine-object collision is avoided. Such planning can be achieved by the convexification method, also called parabolic relaxation [22], differential evolution algorithms based on kinematic constraints [23, 24], Lyapunov stability theory [25], vertical plane underactuated manipulator control, Differential Evolution Optimization (DEO) algorithms supported by an applied robot operating system [26], PID control, differential evolution algorithm [27], among other. Each manipulator robot requires a different approach according to the function. However, ROS is widely used in robotics due to the ease of executing its algorithms to perform movements, object tracking, recognition, and segmentation, among others [11].

III. Materials and Methods

In the first instance, the sketch of the manipulator robot is made to define the 5 DOFs. After that, the robot's inverse kinematics is developed to determine the robot manipulator's kinematic parameters. In Fig. 1, the x_i, y_i and z_i axes are the three-dimensional plane, where the subscript i assumes values of the quantity of the number of joints. Additionally, a_i is denoted as the distance from the axis z_i along the axis x_i. The angle to be rotated z_{i-1} to get to z_i, rotating around x_i is known as α_i. While the distance from the system $x_0y_0z_0$ until the intersection of z_{i-1} toward z_i, throughout z_{i-1} is known as d_i, and the angle from x_{i-1} until x_i spinning around z_i is known as θ_i.

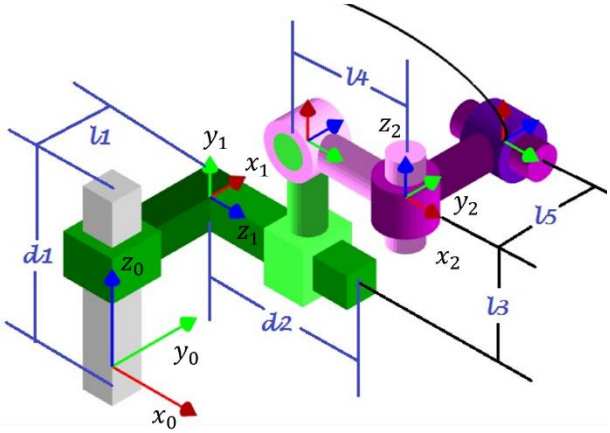

Fig. 1. Kinematic parameters.

Table I shows the kinematic parameters of the robot to apply the Denavit-Hartenberg algorithm.

TABLE I. Parameters Denavit-Hartenberg

i	a_i	α_i	d_i	θ_i
1	L_2	90	Q_1	90
2	L_3	90	Q_2	90
3	L_4	90	0	Q_3
4	L_5	90	0	Q_4
5	L_6	90	0	Q_5

Once this is done, the homogeneous transformation matrices concerning the reference are obtained, multiplying the matrix of each link ${}_{k-1}T^k$ where $k = [1,2,3,\ldots n]$; $n = \#GDL$, Eq. (1). Also, compact expressions are defined as $C\alpha \equiv cos\ (\alpha)$; $S\alpha \equiv sin\ (\alpha)$.

$$
{}_0T^1 = \begin{bmatrix} 0 & 0 & 1 & 0 \\ 1 & 0 & 0 & L_2 \\ 0 & 1 & 0 & d_1 \\ 0 & 0 & 0 & 1 \end{bmatrix}
$$

$$
{}_1T^2 = \begin{bmatrix} 0 & 0 & 1 & L_3 \\ 1 & 0 & 0 & d_2 \\ 0 & 1 & 0 & 0 \\ 0 & 0 & 0 & 1 \end{bmatrix}
$$

$$
{}_2T^3 = \begin{bmatrix} C_3 & 0 & S_3 & L_4 \times C_3 \\ S_3 & 0 & -C_3 & L_4 \times S_3 \\ 0 & 1 & 0 & 0 \\ 0 & 0 & 0 & 1 \end{bmatrix}
$$

$$
{}_3T^4 = \begin{bmatrix} C_4 & 0 & S_3 & L_5 \times C_3 \\ S_4 & 0 & -C_4 & L_5 \times S_3 \\ 0 & 1 & 0 & 0 \\ 0 & 0 & 0 & 1 \end{bmatrix}
$$

$$
{}_4T^5 = \begin{bmatrix} C_5 & 0 & S_5 & L_6 \times C_3 \\ S_5 & 0 & -C_5 & L_6 \times S_3 \\ 0 & 1 & 0 & 0 \\ 0 & 0 & 0 & 1 \end{bmatrix} \quad (1)
$$

The general homogeneous transformation matrix that relates the referential $x_3y_3z_3$ concerning the referential $x_0y_0z_0$ is defined in Eq. (2):

$$ {}_0T^5 = {}_0T^1 \times {}_1T^2 \times {}_2T^3 \times {}_3T^4 \times {}_4T^5 \quad (2) $$

Then, the inertia tensors of the elements that constitute the system are developed concerning their referential transferred to their centers of mass, being I_k the inertia tensors of the system elements, where $k = [1, 2, 3 \dots]$.

$$ D_1(q) = \begin{bmatrix} I_{1_{xx}} + I_{2_{zz}} & 0 & 0 \\ 0 & I_{1_{zz}} + I_{2_{xx}} & 0 \\ 0 & 0 & I_{1_{xx}} + I_{2_{zz}} \end{bmatrix} \quad (3) $$

$$ D_2(q) = \begin{bmatrix} I_{3_{xx}} + I_{4_{zz}} & 0 & 0 \\ 0 & I_{3_{zz}} + I_{4_{xx}} & 0 \\ 0 & 0 & I_{3_{xx}} + I_{4_{xx}} \end{bmatrix} $$

$$ D_3(q) = \begin{bmatrix} I_{5_{zz}} & 0 & 0 \\ 0 & I_{5_{xx}} & 0 \\ 0 & 0 & I_{5_{xx}} \end{bmatrix} $$

$$ D_4(q) = \begin{bmatrix} I_{6_{zz}} & 0 & 0 \\ 0 & I_{6_{xx}} & 0 \\ 0 & 0 & I_{6_{xx}} \end{bmatrix} $$

$$ D_5(q) = \begin{bmatrix} I_{7_{zz}} & 0 & 0 \\ 0 & I_{7_{xx}} & 0 \\ 0 & 0 & I_{7_{xx}} \end{bmatrix} $$

It should be emphasized that the system's total inertia tensors with respect to the axes of rotation or translation relative to the referential base are obtained by adding the tensors of each element.

$$ D(q) = D_1(q) + D_2(q) + D_3(q) + D_4(q) + D_5(q) \quad (4) $$

Eq. (5) is expressed as:

$$ D(q) = \begin{bmatrix} d_{11}(q) & 0 & 0 \\ 0 & d_{22}(q) & 0 \\ 0 & 0 & d_{33}(q) \end{bmatrix} \quad (5) $$

It is worth noting that the system considers the use of gravity in the trajectory equations and the torque of the electric motor in the dynamics of the robot manipulator. If this is not considered, it will affect matrix D, converting it to a 4×3 matrixor a square matrix with many zeros in its components, causing collisions in the joints of the robot.

$$ D_q = \begin{bmatrix} d_{11}(q) & 0 & 0 \\ 0 & d_{22}(q) & 0 \\ 0 & 0 & d_{33}(q) \\ 0 & 0 & 0 \end{bmatrix} \quad (6) $$

$$ D_q = \begin{bmatrix} d_{11}(q) & 0 & 0 \\ 0 & 0 & 0 \\ 0 & 0 & 0 \end{bmatrix} \quad (7) $$

Consequently, we define the vectors from the base referential origin to the center of mass of each element. This is respectively described as:

$$ J_{V1} = \begin{bmatrix} 0 & 0 & 0 & 0 & 0 \\ 0 & 0 & 0 & 0 & 0 \\ 1 & 0 & 0 & 0 & 0 \end{bmatrix} $$

$$ J_{V2} = \begin{bmatrix} 0 & 1 & 0 & 0 & 0 \\ 0 & 0 & 0 & 0 & 0 \\ 1 & 0 & 0 & 0 & 0 \end{bmatrix} \quad (8) $$

$$ J_{V3} = \begin{bmatrix} 0 & 1 & \frac{(\mathrm{L_4C_3})}{2} & 0 & 0 \\ 0 & 0 & 0 & 0 & 0 \\ 1 & 0 & \frac{-(\mathrm{L_4S_3})}{2} & 0 & 0 \end{bmatrix} $$

$$ JV4 = \begin{bmatrix} 0 & 1 & L_4C_3 + \frac{(L_5C_3C_4)}{2} & \frac{-(L_5S_3S_4)}{2} & 0 \\ 0 & 0 & 0 & \frac{(L_5C_4)}{2} & 0 \\ 1 & 0 & -L_4S_3 - \frac{(L_5C_4S_3)}{2} & \frac{-(L_5C_3S_4)}{2} & 0 \end{bmatrix} $$

$$ JV5 = \begin{bmatrix} 0 & 1 & \frac{(L_6 \times (S_3S_5 + C_3C_4C_5))}{2} & d_{14} & d_{15} \\ 0 & 0 & 0 & d_{24} & d_{25} \\ 1 & 0 & L_6C_3S_5 - L_4S_3 - L & d_{34} & d_{35} \end{bmatrix} $$

Then, we define the dynamic equation of the electric motor. We analyze the mechanical subsystem (Fig. 2) and the electrical subsystem (Fig. 3).

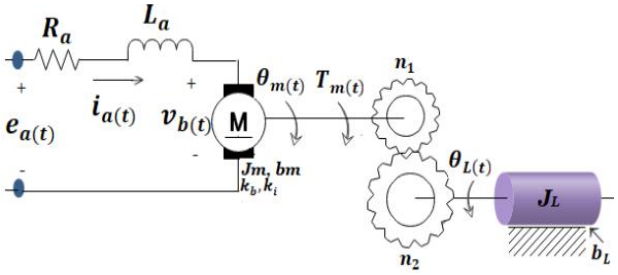

Fig. 2. Mechanical subsystem [28].

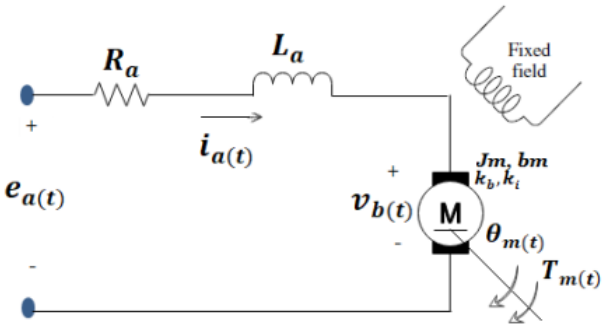

Fig. 3. Electrical subsystem [28].

Starting from Fig. 2, we define the following Eq. (9), where j_m: polar moment of inertia of the motor, b_m:

engine biscose coefficient, $\ddot{\theta}_m$: acceleration, $\dot{\theta}_m$: speed y, w_m: instantaneous angular velocity.

$$\begin{aligned}\tau_T\,(t) &= \tau_m(t) + n\tau_L\,(t) + \tau_N(t)\\ \tau_m(t) &= J_m\ddot{\theta}_m(t) + B_m\dot{\theta}_m(t)\\ \tau_T(t) &= J_m\ddot{\theta}_m(t) + B_m\dot{\theta}_m(t) + n\tau_L(t) + \tau_N(t) \quad (9)\\ \tau_T(t) &= J_m\,\ddot{\theta}_L(t)/n + B_m\,\dot{\theta}_L(t)/n + n\tau_L(t) + \tau_N(t)\end{aligned}$$

Similarly, from Fig. 3, we define the equations of the electrical system, where k_b: back emf constant, θ_m: motor shaft position, L_m: inductor.

$$\begin{aligned}v_m(t) &= R_m i_m(t) + \frac{L_m d}{dt} i_m(t) + e_b\,(t)\\ v_m(t) &= A \times u(t)\\ A \times u(t) &= R_m i_m(t) + e_b(t);\; L_m \approx 0\end{aligned} \quad (10)$$

Once the mechanical and electrical equations are obtained, we perform the electromechanical coupling Eq. (11).

$$\begin{aligned}e_b(t) &= K_b\dot{\theta}_m(t)\\ \tau_T(t) &= K_m i_m(t)\end{aligned} \quad (11)$$

From Eqs. (9)–(12), we obtain the dynamic equation of the electric motor.

$$\begin{aligned}\mu_i = \frac{Rm_i \times Jm_i}{A_i \times Km_i \times n_i}\ddot{q}_i + \left(\frac{Rm_i \times Fm_i}{A_i \times Km_i \times n_i} + \frac{Kb_i}{A_i \times n_i}\right)\dot{q}_i\\ + \frac{Rm_i \times n_i}{A_i}T_i\end{aligned} \quad (12)$$

Eq. (12) as a function of T_i and considering $n_i = 1$, Since the motors do not have reduction gears, the following is obtained:

$$\begin{aligned}T_i = \frac{A_i}{Rm_i} \times u_i - \left[\left(\frac{Jm_i}{Km_i}\right)\ddot{q}_i\right.\\ \left. + \frac{Fm_i + Kb_i \times Rm_i \times Km_i}{Km_i}\dot{q}_i\right]\end{aligned}$$

The total inertia tensors determine the robot's kinetic energy and potential energy.

$$E_c(q,\dot{q}) = \frac{1}{2}(\dot{q}^T \times D(q) \times \dot{q}) \quad (13)$$

$$\begin{aligned}Ec = dq_2 \times ((dq_3 \times (&\frac{L_4 \times M_5 \times cos(q_3)}{2}\\ &+ L_4 \times M_6 \times cos(q_3)\\ &+ L_4 \times M_7 \times cos(q_3)\\ &+ \frac{L_5 \times M_6 \times cos(q_3) \times cos(q_4)}{2}\\ &+ L_5 \times M_7 \times cos(q_3) \times cos(q_4)\\ &+ \frac{(L_6 \times M_7 \times sin(q_3) \times sin(q_5))}{2}\end{aligned}$$

$$\begin{aligned}E_p(q) = -g^T((M_1 + M_2)\overline{C_1}(q) + (M_3 + M_4)\overline{C_2}(q)\\ + M_5\overline{C_3}(q) + M_6\overline{C_4}(q) + M_7\overline{C_5}(q)\end{aligned} \quad (14)$$

$$\begin{aligned}Ep = gr \times (&M_1 \times d_1 - \frac{M_2 \times a_1}{2} - \frac{M_1 \times a_1}{2} + M_2 \times d_1\\ &+ M_3 \times d_1 + M_4 \times d_1 + M_5 \times d_1\\ &+ M_6 \times d_1 + M_7 \times d_1 + \frac{L_3 \times M_3}{2}\\ &+ \frac{L_3 \times M_4}{2} + L_3 \times M_5 + L_3 \times M_6\\ &+ L_3 \times M_7 + \frac{L_4 \times M_5 \times cos(q_3)}{2}\\ &+ L_4 \times M_6 \times cos(q_3)\end{aligned}$$

Finally, the dynamic coupling of the electric motor with the dynamics of the 5 DOF manipulator robot is performed. To do this, we proceed to perform the dynamics of the robot manipulator.

$$\frac{d}{dt}\frac{\partial}{\partial\dot{q}_i}L(q,\dot{q}) - \frac{\partial}{\partial\dot{q}_i}L(q,\dot{q}) = T_i; 1 \le i \le 5 \quad (15)$$

Once Eq. (15) is obtained, we will couple the dynamics of the electric motor to obtain Eqs. (16)–(20), which determine the trajectories of each joint.

$$\begin{aligned}u_{1(t)} = \frac{Rm_1 Jm_1}{A_1 Km_1 n_1}\ddot{q}_1 + \left(\frac{Rm_1 Bm_1}{A_1 Km_1 n_1} + \frac{Kb_1}{A_1 n_1}\right)\dot{q}_1\\ + \left(\frac{n_1 Rm_1}{A_1 Km_1}\right) * ([d_{11}(q)]\ddot{q}_1\\ + [d_{12}(q)]\ddot{q}_2 + [d_{13}(q)]\ddot{q}_3\\ + [d_{14}(q)]\ddot{q}_4 + [d_{15}(q)]\ddot{q}_5 + c_1(q,\dot{q})\\ + h_1(q) + b_1(\dot{q}_1))\end{aligned} \quad (16)$$

$$\begin{aligned}u2(t) = \frac{Rm_2 Jm_2}{A_2 Km_2 n_2}\ddot{q}_2 + \left(\frac{Rm_2 Bm_2}{A_2 Km_2 n_2} + \frac{Kb_2}{A_2 n_2}\right)\dot{q}_2\\ + \left(\frac{n_2 Rm_2}{A_2 Km_2}\right) \times ([d_{21}(q)]\ddot{q}_1\\ + [d_{22}(q)]\ddot{q}_2 + [d_{23}(q)]\ddot{q}_3\\ + [d_{24}(q)]\ddot{q}_4 + [d_{25}(q)]\ddot{q}_5 + c_2(q,\dot{q})\\ + h_2(q) + b_2(\dot{q}_2))\end{aligned} \quad (17)$$

$$\begin{aligned}u_3(t) = \frac{Rm_3 Jm_3}{A_3 Km_3 n_3}\ddot{q}_3 + \left(\frac{Rm_3 Bm_3}{A_3 Km_3 n_3} + \frac{Kb_3}{A_3 n_3}\right)\dot{q}_3\\ + \left(\frac{n_3 Rm_3}{A_3 Km_3}\right) \times ([d_{31}(q)]\ddot{q}_1\\ + [d_{32}(q)]\ddot{q}_2 + [d_{33}(q)]\ddot{q}_3\\ + [d_{34}(q)]\ddot{q}_4 + [d_{35}(q)]\ddot{q}_5 + c_3(q,\dot{q})\\ + h_3(q) + b_3(\dot{q}_3))\end{aligned} \quad (18)$$

$$\begin{aligned}u_4(t) = \frac{Rm_4 Jm_4}{A_4 Km_4 n_4}\ddot{q}_4 + \left(\frac{Rm_4 Bm_4}{A_4 Km_4 n_4} + \frac{Kb_4}{A_4 n_4}\right)\dot{q}_4\\ + \left(\frac{n_4 Rm_4}{A_4 Km_4}\right) \times ([d_{41}(q)]\ddot{q}_1\\ + [d_{43}(q)]\ddot{q}_2 + [d_{43}(q)]\ddot{q}_3\\ + [d_{44}(q)]\ddot{q}_2 + [d_{45}(q)]\ddot{q}_3 + c_4(q,\dot{q})\\ + h_4(q) + b_4(\dot{q}_4))\end{aligned} \quad (19)$$

$$\begin{aligned}u_5(t) = \frac{Rm_5 Jm_5}{A_5 Km_5 n_5}\ddot{q}_5 + \left(\frac{Rm_5 Bm_5}{A_5 Km_5 n_5} + \frac{Kb_5}{A_5 n_5}\right)\dot{q}_5\\ + \left(\frac{n_5 Rm_5}{A_5 Km_5}\right) \times ([d_{51}(q)]\ddot{q}_1\\ + [d_{53}(q)]\ddot{q}_2 + [d_{53}(q)]\ddot{q}_3\\ + [d_{53}(q)]\ddot{q}_4 + [d_{53}(q)]\ddot{q}_5 + c_5(q,\dot{q})\\ + h_5(q) + b_5(\dot{q}_5))\end{aligned}$$

Once the mathematical part is finished, the manipulator robot is modeled using Autodesk Inventor software (Fig. 4). The construction material chosen is 316 stainless steel for its suitability for handling food products. This material offers high resistance to non-oxidizable acids and pitting corrosion and a moderate aesthetic level.

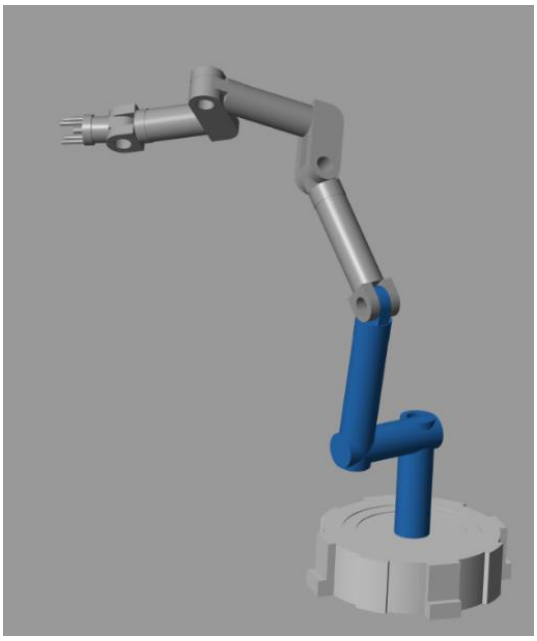

Fig. 4. Robot manipulator.

On the other hand, the code to execute the trajectories of the robot manipulator is developed. Through a flowchart (Fig. 5), an overview of the operation of the manipulator robot is shown.

Subsequently, the code of the manipulator robot is made. For this, essential code fragments for executing the robot manipulator are detailed. Table II shows the dimensions of each link (d_i), the speeds of each joint (dq_i), and execution time of the 5 GL robot (t_i).

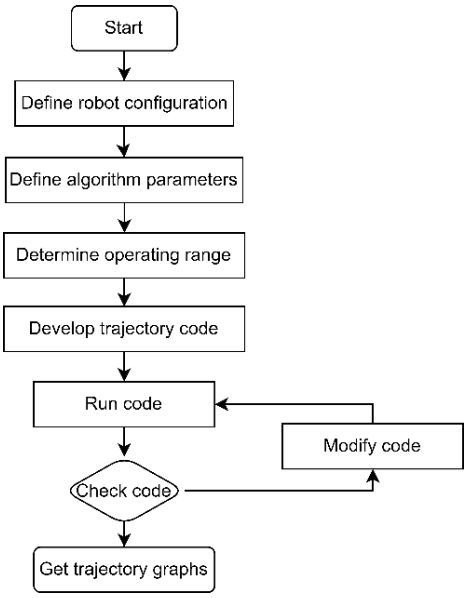

Fig. 5. Operation flow of the manipulator robot.

TABLE II. KINEMATIC PARAMETERS

Kinematic Parameters			
i	***d***	dq_i	t_i
1	q_1=-105	dq_1=4	t_1=0
2	q_2=65	dq_2=3	t_2=10
3	q_3=150	dq_3=6	t_3=20
4	q_4=45	dq_4=3	t_4=30
5	q_5=90	dq_5=2	t_5=40
6	q_6=55	dq_6=1	t_6=50
7	q_7=90	dq_7=0.5	t_7=60

IV. RESULTS

After executing the program, the joint movement of the robot manipulator is obtained as a result. In Fig. 6, the robot can be seen performing the lifting movement. The joint qv_2 and qv_5 perform a translation in the z-axis and the joint qv_3 on the y-axis.

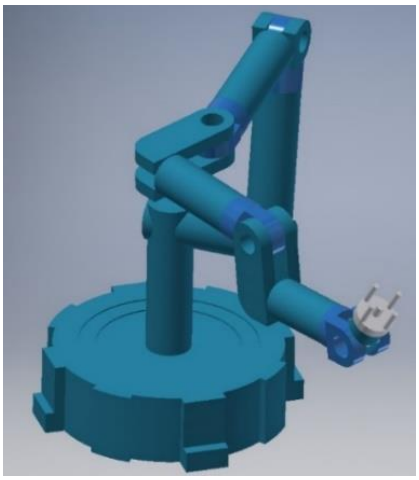

Fig. 6. Robot manipulator lifting movement

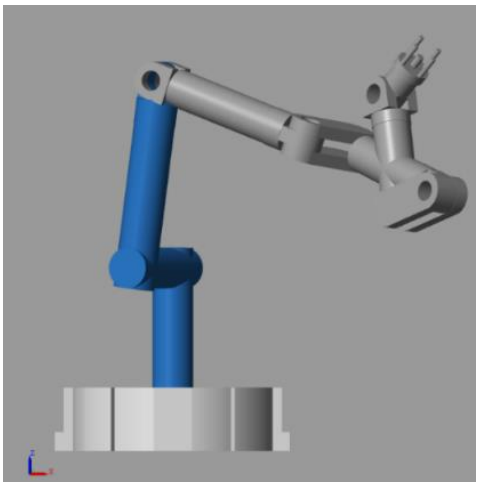

Fig. 7. Emptying movement of the manipulator robot.

Fig. 7 shows the emptying movement of the manipulator robot. In this image the joints qv_4 and qv_5 performs a translation in the x axis, to be able to tilt the hook of the manipulator robot.

However, each joint presents its own trajectory, however, q_1 (Fig. 8(a)), q_2 (Fig. 8(b)), q_4 (Fig. 8(d)) and

q_6 (Fig. 8(f)) have a similarity in terms of their trajectory, more not at runtime. Similarly, joints q_3 (Fig. 8(c)) and q_5 (Fig. 8(e)). It should be emphasized that the last 2 joints have an inverse trajectory to q_1.

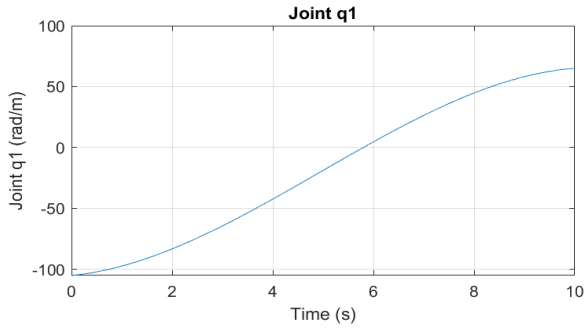

(a)

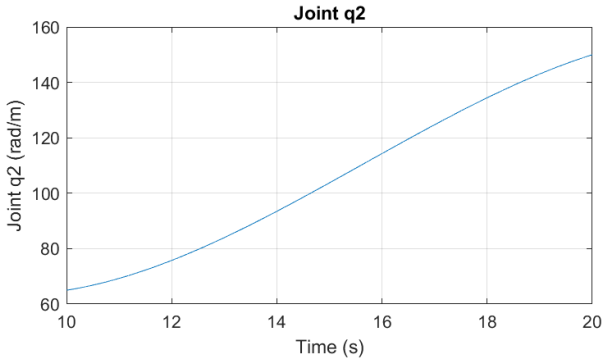

(b)

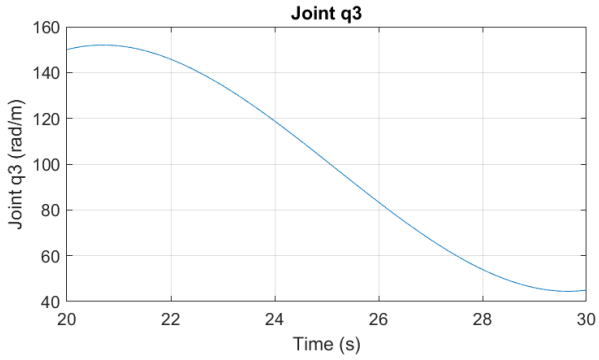

(c)

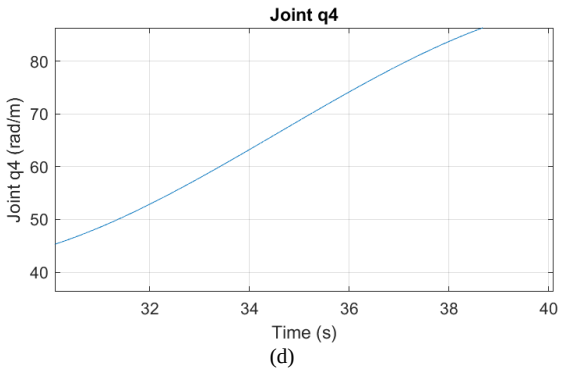

(d)

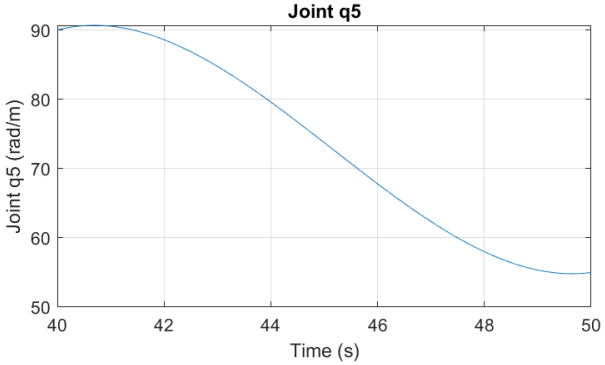

(e)

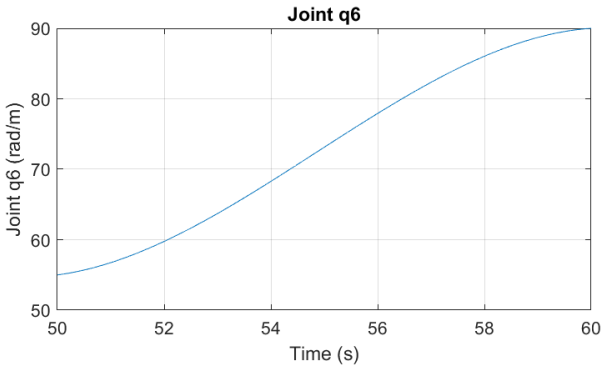

(f)

Fig. 8. Joint trajectory (a) q_1, (b) q_2, (c) q_3, (d) q_4, (e) q_5 and (f) q_6.

In addition, the total angular displacement is acquired (Fig. 9(a)), to illustrate the overall angular rotation of the robot manipulator. The graphs of the total angular velocity (Fig. 9(b)) and the total acceleration (Fig. 9(c)) are also derived.

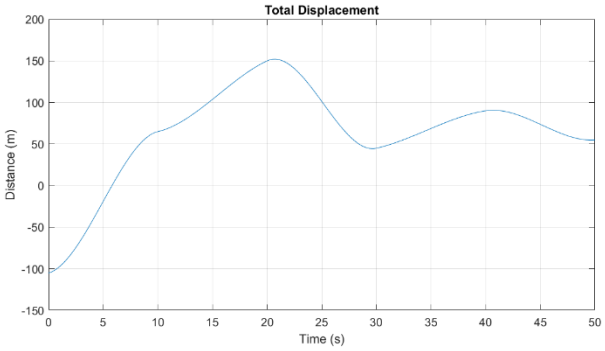

(a)

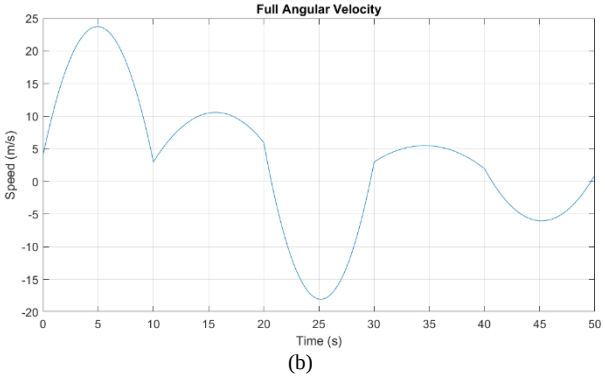

(b)

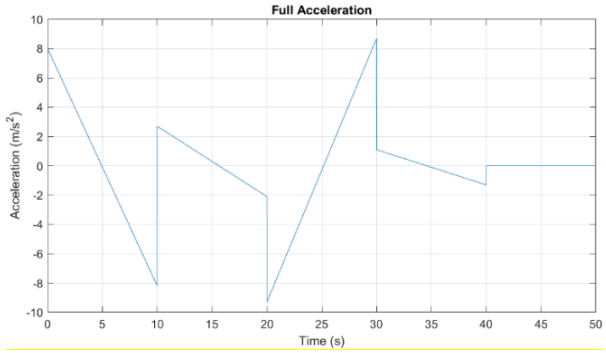

(c)

Fig. 9. Full (a) angular displacement, (b) Full angular velocity and (c) Full acceleration.

To visualize the execution of the joints of the manipulator robot, we go to the following link: https://n9.cl/5qdo6. On the other hand, we use the Matlab tuner to design the PID controller. For this, we define the transfer functions of the joints to be controlled. After that, we apply the tuner and obtain the controller parameters expressed in Table III.

TABLE III. CONTROLLER PARAMETERS PID

Parameter	Value
K_p	65.6122
K_i	5.548
K_d	23.491

In Fig. 10, we have the graph of the angular positions of the joints $q_1(t)$, $q_2(t)$, $q_3(t)$ and $q_4(t)$ using the PID controller. We see that at approximately 4 s, the joints of the robot manipulator come to stabilization.

However, the robot manipulator is prone to both external and internal disturbances. The torque exerted by the motor is crucial for this type of robot. For this, a robust PID controller would be the most appropriate excellent due to its great control against disturbances such as torque. However, from the present work, we can change the type of control to a predictive control, relying on neural networks and artificial intelligence, to obtain a robot manipulator that can predict with total certainty other types of movements at different ranges and with absolute precision, in addition to constantly feedback from each execution.

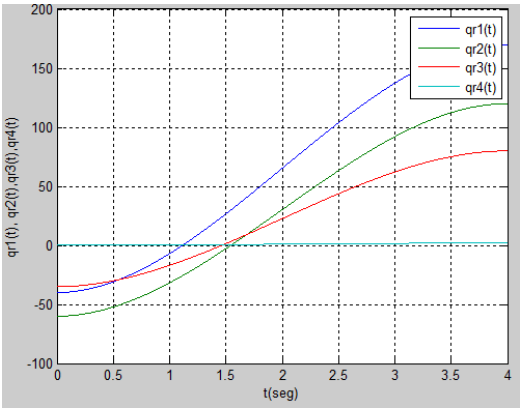

Fig. 10. Angular positions with PID control.

V. CONCLUSIONS

In analyzing the robot manipulator's dynamics, it is essential to consider the influence of gravity. This consideration is directly associated with the centers of inertia of each joint, which, in turn, are connected to the overall inertia tensors. Neglecting this factor could result in collisions between the robot's various components.

With the developed program, it was shown that the articulations q_1 (Fig. 8(a), q_2 (Fig. 8(b), q_4 (Fig. 8(d), and q_6 (Fig. 8(f) present a similar trajectory, but with different execution times. On the other hand, joints q_3 (Fig. 8(c) and q_5 (Fig. 8(e) show an inverse trajectory to the first four joints but with the same characteristics described.

In Fig. 9(b) and Fig. 9(c), the maximum angular velocity and maximum angular acceleration can be seen, with values of $24\ m/s$ to $-18\ m/s$ and from $-20\ m/s^2$ to $8\ m/s^2$ respectively. These values enable us to make an appropriate choice for the electric motor for the robot manipulator.

The PID control elaborated based on the tuning in Matlab, was adequate but not optimal because the stabilization of the joints reaches approximately 4 s (Fig. 10), which, in that period the robot is ready for disturbances that would crucially affect the future functions to be performed. Additionally, further investigation can focus on optimizing PID control for faster joint stabilization and reduced vulnerability to disturbances.

CONFLICT OF INTEREST

The authors declare no conflict of interest.

AUTHOR CONTRIBUTIONS

EP conducted the research; RA analyzed the data; HP wrote the paper; EP reviewed the manuscript; all authors had approved the final version.

REFERENCES

[1] A. L. Sánchez, "Debates on digitization and robotization of (human) work of the future: Replacing automation, technological pragmatism, augmentation and heteromation," *Revista Española de Sociología*, vol. 30, no. 3, a66, Jul. 2021.

[2] P. Gan, P. Li, H. Xia, X. Zhou, and X. Tang, "The application of artificial intelligence in improving colonoscopic adenoma detection rate: Where are we and where are we going," *Gastroenterol Hepatol*, vol. 46, no. 3, pp. 203–213, Mar. 2023

[3] J. A. D. Rosa *et al.*, "Artificial intelligence in the simulation of fungicide management scenarios for satisfactory yield and food safety in oat crops," *Social and Environmental Management Magazine*, vol. 17, no. 1, e03161, Feb. 2023.

[4] H. A. Moreno, R. Saltaren, I. Carrera, L. Puglisi, and R. Aracil, "Performance indices of manipulator robots: A state-of-the-art review," *Ibero-American Magazine of Automation and Industrial Computing RIAI*, vol. 9, no. 2, pp. 111–122, Apr. 2012. (in Spainsh)

[5] O. D. Zabaleta Laverde, "Construction and position control of a robotic arm prototype of two degrees of freedom," *Habitus Magazine: Research hotbeds*, no. 3, pp. 92–101, Sep. 2012. (in Spainsh)

[6] Y. Bouteraa, I. Ben Abdallah, K. Alnowaiser, M. R. Islam, A. Ibrahim, and F. Gebali, "Design and development of a smart IoT-based robotic solution for wrist rehabilitation," *Micromachines (Basel)*, vol. 13, no. 6, 973, Jun. 2022.

[7] A. Acuna *et al.*, "Design and validation of a modular micro-robotic system for the mechanical characterization of soft tissues," *Acta Biomater*, vol. 134, pp. 466–476, Oct. 2021.
[8] N. Pinrath and N. Matsuhira, "Development of a real-time simulator for a semi-autonomous tele-robot in an unknown narrow path," *Journal of Robotics and Mechatronics*, vol. 34, no. 3, pp. 631–644, Jun. 2022.
[9] N. Igo *et al.*, "Robots climbing up and down a steep stairs and robots retrieving objects from high places," *Journal of Robotics and Mechatronics*, vol. 34, no. 3, pp. 509–522, Jun. 2022.
[10] Z. Yuan *et al.*, "Safe-control-gym: A unified benchmark suite for safe learning-based control and reinforcement learning in robotics," *IEEE Robot Autom Lett*, vol. 7, no. 4, pp. 11142–11149, Oct. 2022.
[11] T. Fischer, W. Vollprecht, S. Traversaro, S. Yen, C. Herrero, and M. Milford, "A robostack tutorial: Using the robot operating system alongside the conda and jupyter data science ecosystems," *IEEE Robot Autom Mag*, vol. 29, no. 2, pp. 65–74, Jun. 2022.
[12] F. Zhou *et al.*, "Electromechanical model-based adaptive control of multilayered dielectric elastomer bending actuator," *J Appl Mech*, vol. 88, no. 11, Nov. 2021.
[13] B. Weng, H. Chen, and W. Zhang, "On the convergence of multi-robot constrained navigation: A parametric control lyapunov function approach," in *Proc. 2022 International Conference on* Robotics *and Automation (ICRA)*, IEEE, May 2022, pp. 4972–4978.
[14] R. J. Yahya and N. H. Abbas, "Optimal integral sliding mode controller controller design for 2-RLFJ manipulator based on hybrid optimization algorithm," *International Journal of Electrical and Computer Engineering (IJECE)*, vol. 12, no. 1, p. 293, Feb. 2022.
[15] R. Herguedas, M. Aranda, G. Lopez-Nicolas, C. Sagucs, and Y. Mezouar, "Multirobot control with double-integrator dynamics and control barrier functions for deformable object transport," in *Proc 2022 International* Conference *on Robotics and Automation (ICRA)*, IEEE, May 2022, pp. 1485–1491.
[16] I. Clitan, C. Stancioi, and V. Muresan, "Predictive motor speed control for an industrial robot, a dead-beat approach," in *Proc. International* Conference *on Reliable Systems Engineering (ICoRSE) - 2021*, 2022, pp. 278–286.
[17] M. A. Najafqolian, K. Alipour, R. Mousavifard, and B. Tarvirdizadeh, "Formation control of multiple aerial robots using LSTM-based model predictive control," in *Proc. 2022 10th RSI International Conference on Robotics and Mechatronics (ICRoM)*, IEEE, Nov. 2022, pp. 401–407.
[18] Y. J. Pak, Y. S. Kong, and J. S. Ri, "Robust PID optimal tuning of a delta parallel robot based on a hybrid optimization algorithm of particle swarm optimization and differential evolution," *Robotica*, vol. 41, no. 4, pp. 1159–1178, Apr. 2023.
[19] F. Dib, N. Benaya, K. B. Meziane, and I. Boumhidi, "Comparative study of optimal tuning PID controller for manipulator robot," in *Proc. International Conference on Smart City Applications, SCA 2022*, 2023, vol. 6, pp. 252–261.
[20] Y. H. T. Htun, M. S. Hlaing, and T. T. Hla, "Master-slave synchronization of robotic arm using PID controller," *Indonesian* Journal *of Electrical Engineering and Informatics (IJEEI)*, vol. 11, no. 1, Jan. 2023.
[21] J. Han, X. Shan, H. Liu, J. Xiao, and T. Huang, "Fuzzy gain scheduling PID control of a hybrid robot based on dynamic characteristics," *Mech Mach Theory*, vol. 184, 105283, Jun. 2023.
[22] C. Choi, M. Adil, A. Rahmani, and R. Madani, "Multi-robot motion planning via parabolic relaxation," *IEEE Robot Autom Lett*, vol. 7, no. 3, pp. 6423–6430, Jul. 2022.
[23] L. Wang, X. Lai, P. Zhang, and M. Wu, "A control strategy based on trajectory planning and optimization for two-link Underactuated manipulators in vertical plane," *IEEE Trans Syst Man Cybern Syst*, vol. 52, no. 6, pp. 3466–3475, Jun. 2022.
[24] L. Qiao, X. Luo, and Q. Luo, "Control of trajectory tracking for mobile manipulator robot with kinematic limitations and self-collision avoidance," *Machines*, vol. 10, no. 12, 1232, Dec. 2022.
[25] R. A. L. León, C. N. M. Quiroz, D. E. C. Inga, and C. A. P. Cárdenas, "Control algorithm using lyapunov stability for trajectory following and 3D potential fields in obstacle avoidance in an aerial robot," in *Proc. 20th LACCEI International Multi-Conference for Engineering, Education and Technology: "Education, Research and Leadership in Post-pandemic Engineering: Resilient, Inclusive and Sustainable Actions*, Latin American and Caribbean Consortium of Engineering Institutions, 2022, vol. 3.
[26] I. J. Kazim, Y. Tan, and L. Qaseer, "Integration of DE algorithm with PDC-APF for enhancement of contour path planning of a universal robot," *Applied Sciences*, vol. 11, no. 14, 6532, Jul. 2021.
[27] B. Gao, H. Guan, W. Tang, W. Han, and S. Xue, "Research on position recognition and control method of single-leg joint of hydraulic quadruped robot," *Recent Advances in Electrical & Electronic Engineering (Formerly Recent Patents on Electrical & Electronic Engineering)*, vol. 14, no. 8, pp. 802–811, Dec. 2021.
[28] L. F. Obando. Transfer function of the DC motor and its load. [Online]. Available: https://dademuch.com/2019/04/24/funcion-de-transferencia-del-motor-dc-y-su-carga/